# Controlled *p*- and *n*-type doping of $Fe_2O_3$ nanobelt field effect transistors

Zhiyong Fan
*Department of Chemical Engineering and Materials Science, University of California, Irvine, California 92697*

Xiaogang Wen and Shihe Yang
*Department of Chemistry, The Hong Kong University of Science and Technology, Clear Water Bay, Kowloon, Hong Kong*

Jia G. Lu[a)]
*Department of Chemical Engineering and Materials Science and Department of Electrical Engineering and Computer Science, University of California, Irvine, California 92697*

(Received 28 March 2005; accepted 23 May 2005; published online 1 July 2005)

Pure $\alpha$-$Fe_2O_3$ nanobelts are configured as field effect transistors and electrical transport studies demonstrate their *n*-type behavior. In order to control the electrical properties of the fabricated transistor, the nanobelt channels are doped with zinc. Depending on the doping condition, $\alpha$-$Fe_2O_3$ nanobelts can be modified to either *p*-type or *n*-type with enhanced conductivity and electron mobility. Such behavior change is exhibited in the variation of the current-voltage (*I-V*) and *I-V*$_g$ characteristics. © *2005 American Institute of Physics*. [DOI: 10.1063/1.1977203]

Quasi-one-dimensional materials, such as nanotubes and nanowires, are considered as highly promising nanoscale building blocks for integrated electronic and photonic circuits.[1,2] In this regard, the control of electron and hole doping in these nanostructures is of paramount importance. The doping approach is usually implemented by incorporating impurity elements during the synthesis procedures.[3] In our work, $\alpha$-$Fe_2O_3$ nanobelts are configured as field effect transistors (FETs), followed by a controlled *in situ* doping method using zinc (Zn) as the impurity element to achieve *p*- or enhanced *n*-type semiconducting property. Carrier concentrations and mobilities are obtained from the electrical transport studies. Furthermore, the mechanism of *p*- and *n*-type doping using only one impurity element is discussed.

Large-area vertically aligned $\alpha$-$Fe_2O_3$ nanobelts (as shown in Fig. 1(a)) and nanowires have been successfully synthesized via thermal oxidation of iron substrate under appropriate flow of oxygen. It was observed that there was a morphology transition from nanobelt to nanowire when the synthesis temperature was increased from 400 °C to 800 °C.[4] In this work, the $\alpha$-$Fe_2O_3$ nanobelts grown at 700 °C were configured as FETs in order to characterize their electrical transport properties and also explore their potential application for integrated nanoelectronics. The device fabrication process can be briefly described as follows. The as-synthesized nanobelts suspended in isopropyl alcohol were dropped onto a degenerately doped *p*-type silicon substrate capped with 200 nm oxide layer. Photoresist was then spin-coated onto the substrate, and photolithography was performed to define an array of 100 $\mu m^2$ pads. Finally, 10 nm thick Ni and 100 nm thick Au were evaporated in sequence onto this substrate, forming the electrical contacts to the nanobelts. Individual nanobelt with good contacts on both ends were located with a high magnification optical microscope or scanning electron microscope (SEM), as shown in Fig. 1(b). Consequently, $Fe_2O_3$ nanobelt FETs were obtained with metal contacts functioning as the source and drain electrodes, and Si substrate acting as the back gate, as illustrated in Fig. 1(c).

Electrical transport measurements on nanobelt FETs were conducted under room temperature and ambient condition. Figure 2 demonstrates the typical results for a FET with nanobelt width $a$=80 nm, height $b$=38 nm, and length $L$ =6.4 $\mu$m. From the current-voltage (*I-V*) characteristics [Fig. 2] obtained under gate voltages ($V_g$) -of 10, 0, and 10

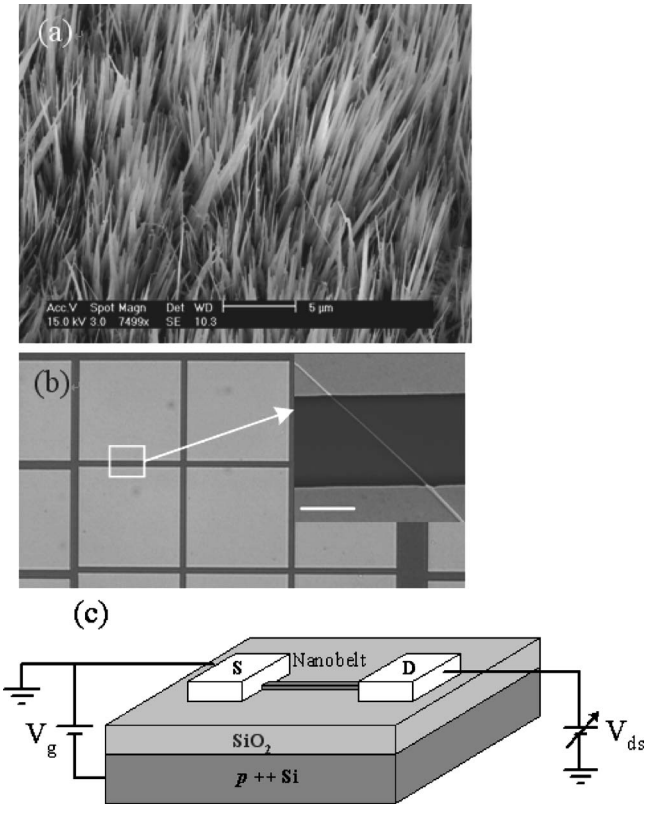


FIG. 1. (a) An array of vertically aligned $\alpha$-$Fe_2O_3$ nanobelts. (b) An individual $\alpha$-$Fe_2O_3$ nanobelt (inset shows the zoomed-in SEM image) is contacted by a pair of the electrode pads. Scale bar: 3 $\mu$m. (c) A schematic of a nanobelt FET with metal contacts functioning as the source and drain electrodes, and Si as the back gate.

[a)]Author to whom correspondence should be addressed; electronic mail: jglu@uci.edu

 

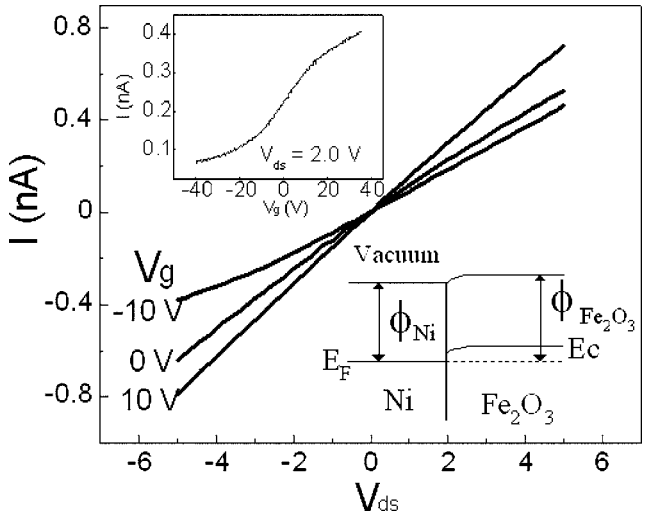


FIG. 2. *I-V* characteristics of an $\alpha$-$Fe_2O_3$ nanobelt FET obtained at back gate potentials of –10 V, 0 V, and 10 V. Bottom inset: Energy band diagram of Ni–$Fe_2O_3$ nanobelt contact, $\phi$ is the work function. Top inset: $I$-$V_g$ curve of the nanobelt FET obtained at 2.0 V drain-source bias.

V, it can be clearly seen that the conductance of the nanobelt increases monotonically as the gate potential increases. This indicates that the as-grown $\alpha$-$Fe_2O_3$ nanobelts are *n*-type semiconductors. In addition, the linearity of the *I-V* curves around $V_{ds}=0$ V suggests that ohmic contacts are formed between Ni and $Fe_2O_3$ nanobelt, which can be attributed to the higher work function of $Fe_2O_3$ (5.4 eV) (Ref. 5) than Ni (5.2 eV), as depicted in the bottom inset of Fig. 2. The pA current level reveals low conductivity of the nanobelts. Considering the geometry of this specific sample with parameters given above, the electrical conductivity $\sigma=2.2\times10^{-3}$ $(\Omega\ \mathrm{cm})^{-1}$ can be estimated from the *I-V* characteristic at $V_g=0$ V. The top inset of Fig. 2 shows the $I$-$V_g$ curve of the nanobelt FET at $V_{ds}=2.0$ V. As is known, the charge carrier concentration and field effect mobility in a typical cylindrical nanowire system with radius $r$ can be expressed as:[6]

$$n=\frac{V_{gt}}{e}\times\frac{2\pi\varepsilon_0\varepsilon_r}{\ln(2h/r)}, \tag{1}$$

$$\mu=\frac{dI}{dV_g}\times\frac{\ln(2h/r)}{2\pi\varepsilon_0\varepsilon_r}\times\frac{L}{V_{ds}}, \tag{2}$$

where $V_{gt}$ is the threshold gate voltage, $e$ is the electron charge, $\epsilon_r$ ($\epsilon_r=3.9$ for $SiO_2$) (Ref. 7) and $h$ are the relative dielectric constant and thickness of gate oxide layer, and $L$ is the channel length, respectively. Although a nanobelt does not have a cylindrical geometry, it is reasonable to estimate the capacitance using $a=2r$ as a first order approximation. $V_{gt}=-27.1$ V and $dI/dV_g=8.2\times10^{-12}$ A/V can be extrapolated from the linear region (-6 V to +6 V) of $I$-$V_g$ curve. Therefore, the electron concentration is estimated to be $n=1.59\times10^{8}$ $\mathrm{cm}^{-1}$, which corresponds to a bulk concentration of $5.3\times10^{18}$ $\mathrm{cm}^{-3}$, and the mobility is calculated to be $\mu_e=2.8\times10^{-3}$ $\mathrm{cm}^2/\mathrm{V\ s}$.

The native *n*-type behavior for semiconducting metal-oxide nanostructures, such as ZnO and $In_2O_3$ nanobelts, has been well documented and attributed to the oxygen vacancies.[6,8] Although in some context, $\alpha$-$Fe_2O_3$ is regarded as a charge-transfer insulator,[9] it tends to be an *n*-type semiconductor in the presence of oxygen vacancies.[10] In addition, $\alpha$-$Fe_2O_3$ has demonstrated its peculiar behavior of the *n*- to *p*-type transition under certain conditions due to its narrower band gap ($E_g=2.2$ eV) compared with $In_2O_3$ ($E_g=3.6$ eV) and ZnO ($E_g=3.4$ eV). This phenomenon has triggered many research interests and is of particular importance for gas sensing study.[10,12] For pure $\alpha$-$Fe_2O_3$, the *n*- to *p*-type transition has been ascribed to the formation of a surface inversion layer due to oxygen adsorption.[10,11] In this work, Zn was introduced into $\alpha$-$Fe_2O_3$ nanobelts as a dopant. It was observed that both *n*- and *p*-type behavior could be achieved stably by controlling the doping conditions.

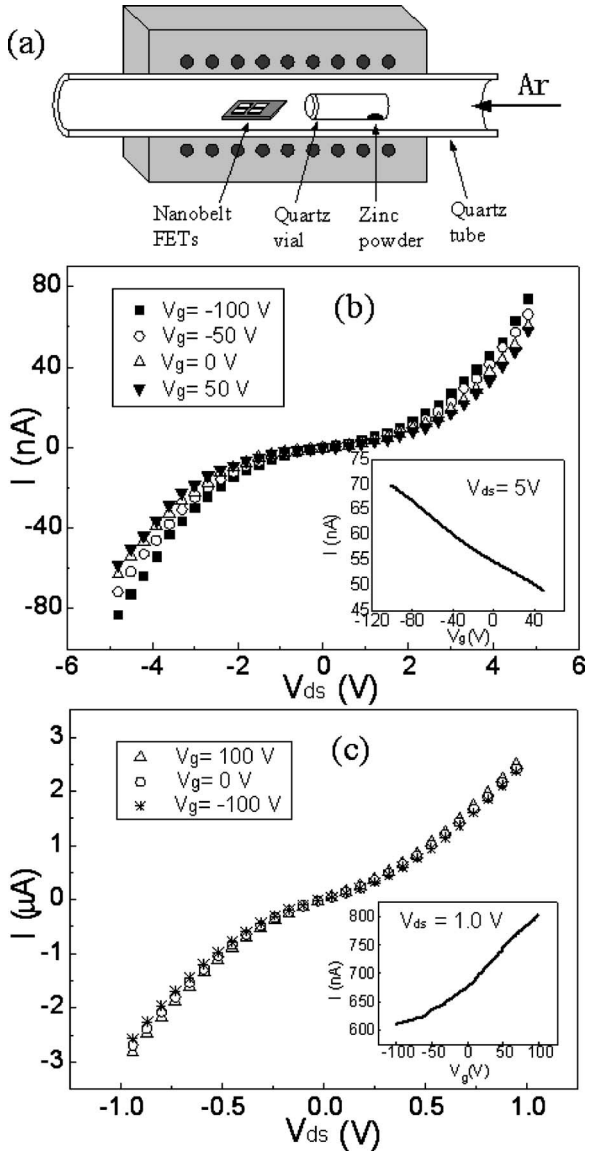


FIG. 3. (a) A schematic of experimental setup for doping $\alpha$-$Fe_2O_3$ nanobelt with Zn source. (b) *I-V* curves and $I$-$V_g$ curve (inset) of the *p*-type $\alpha$-$Fe_2O_3$ nanobelt FETs doped at 700 °C for 5 min. (c) *I-V* curves and $I$-$V_g$ curve (inset) of the enhanced *n*-type $\alpha$-$Fe_2O_3$ nanobelt FETs doped at 350 °C for 1 h.

The doping experiment was carried out inside a thermal furnace, as illustrated in Fig. 3(a). The chip with the nanobelt FETs was placed at the center of the furnace. An openend quartz vial containing a small amount of pure Zn powder (~10 mg, 99.99%, Alfa Aeasar) was placed 12 cm away at upstream. The system was first purged with pure Ar three times to evacuate air, and then maintained in 760 Torr Ar.

During doping, Zn vapor was transported via 100 sccm Ar carrier gas. To obtain *p*-type nanobelts, the furnace temperature at the sample was quickly ramped up to 700 °C in 3 min, and held for 5 min followed by 20 min cooling time. During this process, the highest temperature at Zn source was around 600 °C due to the temperature gradient inside the furnace. The doped nanobelts were then subject to electrical transport measurement, and the typical results are plotted in Fig. 3(b). The typical *I-V* curves and the $I$-$V_g$ curve in Fig. 3(b) suggest that $\alpha$-$Fe_2O_3$ nanobelts have been converted to *p*-type semiconductors, since the increase of gate voltage results in the decrease of channel conductance. In addition, the electrical conductivity increased to $0.27(\Omega\,\mathrm{cm})^{-1}$, which is two orders of magnitude greater than that before Zn doping. Combining Eqs. (1) and (2) and the geometry of this specific nanobelt ( $a=66$ nm, $b=27$ nm, $L=3.9$ $\mu$m), the hole concentration and mobility are estimated to be $p=1.2\times10^{20}\,\mathrm{cm}^{-3}$ and $\mu_p=1.3\times10^{-2}\,\mathrm{cm}^2/\mathrm{V\,s}$, respectively. On the other hand, it was observed that *n*-type $\alpha$-$Fe_2O_3$ nanobelts with enhanced carrier concentration and mobility could be also obtained by using different doping conditions. In this case, doping was conducted at a temperature of 350 °C at the sample substrate, while Zn source temperature was at 250 °C, and the duration for doping was extended to 1 h. Figure 3(c) demonstrates the typical electrical transport results of the nanobelts subjected to such a doping process. The *I-V* curves and the $I$-$V_g$ curve indicate that the nanobelt is an *n*-type semiconductor with much higher conductivity. An estimation of the electrical conductivity gives $\sigma=17.2\,(\Omega\,\mathrm{cm})^{-1}$, which is almost four orders of magnitude higher than that of the nanobelts before doping. In addition, electron concentration and mobility are estimated to be $n=8.9\times10^{19}\,\mathrm{cm}^{-3}$ and $\mu_e=3.2\times10^{-1}\,\mathrm{cm}^2/\mathrm{V\,s}$ for this sample with $a=86$ nm, $b=41$ nm, and $L=2.41$ $\mu$m.

The electrical behavior, *n*- or *p*-type, is attributed to the temperature dependence of the Zn-doping process in $Fe_2O_3$. At low temperature, Zn introduced onto the surface of the nanobelts serves as an electron donor thus contributing to an enhanced *n*-type conductivity, this process is similar to the chemical doping of carbon nanotubes with alkaline metal.[13,14] At high temperature, $Zn^{2+}$ substitutionally replaces $Fe^{3+}$, consequently increases hole concentration, giving rise to *p*-type behavior. As shown in the experiments, doping of $\alpha$-$Fe_2O_3$ nanobelts with Zn does not require a very high temperature and long time as compared with doping bulk $\alpha$-$Fe_2O_3$ with Magnesium (Mg).[15] This can be reasoned by considering two facts: (1) Zn has smaller atomic radius ($R_{Zn}=0.142$ nm) than Mg ($R_{Mg}=0.145$ nm) and Fe ($R_{Fe}=0.156$ nm), which renders higher diffusivity of Zn in the $\alpha$-$Fe_2O_3$ lattice; and (2) a nanobelt has a large surface-to-volume ratio, which makes the diffusion from the surface of the sample a more significant effect.

The doping effect on the transition to *p*-type or enhanced *n*-type behavior also manifests itself in the modification of the contact property, as observed in the increasingly nonlinear *I-V* curves shown in Fig. 3. As mentioned before, the roek function of undoped $Fe_2O_3$ is slightly larger than the Ni electrode, thus the linear *I-V* curves [Fig. 2] indicate that the ohmic contacts are formed between the electrode and the nanobelt. As the sample is compensation doped to *p*-type, the Fermi level ($E_F$) approaches the top of the valence band ($E_V$), thus the work function of the *p*-type $Fe_2O_3$ nanobelt is significantly increased, yielding a large Schottky barrier for hole transport as depicted in Fig. 4(a), and pronounced nonlinearity in *I-V* characteristics shown in Fig. 3(b). On the other hand, as the sample is doped with more donors showing enhanced *n*-type behavior, the Fermi level in the $Fe_2O_3$ nanobelt shifts readily toward the conduction band ($E_C$), thus the work function of the sample decreases to be smaller than that of the Ni electrode, yielding the Schottky contact for electron transport [Fig. 4(b)] and nonlinearity of *I-V* characteristics [Fig. 3(c)].

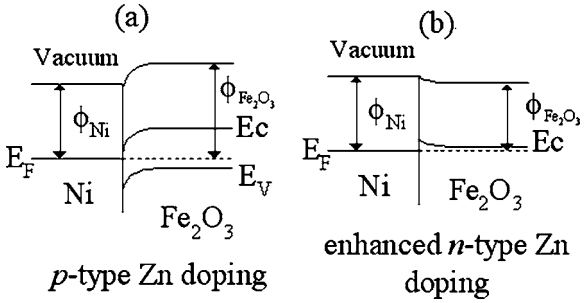


FIG. 4. Energy band diagrams of Ni–$Fe_2O_3$ nanobelt contact for (a) *p*-type Zn doping and (b) enhanced *n*-type Zn doping.

In summary, controlled *p*- and *n*-type doping of $\alpha$-$Fe_2O_3$ nanobelts with Zn as a dopant was achieved. Electrical transport investigations demonstrate enhanced charge carrier concentration and mobility. With both *p*- and *n*-channel FETs fabricated, $Fe_2O_3$ nanomaterials can be utilized as potential building blocks for future nanoscale electronic and magnetoelectronic devices.

The authors thank Dr. Po-Wen Chiu at the Max-Planck Institute for Solid-State Research for valuable discussions. Device fabrication was done at UC Irvine Integrated Nanosystems Research Facility. This work was supported by the NSF Grant No. ECS-0306735 and EEC-0210120.

[1] X. Liu, C. Lee, C. Zhou, and J. Han, Appl. Phys. Lett. **79**, 3329 (2001).
[2] C. J. Barrelet, A. B. Greytak, and C. M. Lieber, Nano Lett. **4**, 1981 (2004).
[3] Y. Cui, X. Duan, J. Hu, and C. M. Lieber, J. Phys. Chem. B **104**, 5213 (2000).
[4] X. Wen, S. Wang, Y. Ding, Z. L. Wang, and S. Yang, J. Phys. Chem. B **109**, 215 (2005).
[5] V. E. Hendrich and P. A. Cox, *Surface Science of Metal Oxides* (Cambridge University Press, Cambridge, UK, 1994).
[6] Z. Fan, D. Wang, P. Chang, W. Tseng, and J. G. Lu, Appl. Phys. Lett. **85**, 5923 (2004).
[7] S. M. Sze, *Modern Semiconductor Device Physics* (Wiley, New York, 1998).
[8] B. Lei, C. Li, D. Zhang, T. Tang, and C. Zhou, Appl. Phys. A: Mater. Sci. Process. **79**, 439 (2004).
[9] G. Dräger and W. Czolbe, Phys. Rev. B **45**, 8283 (1992).
[10] A. Gurlo, M. Sahm, A. Oprea, N. Barsa, and U. Weimar, Sens. Actuators B **102**, 291 (2004).
[11] A. Gurlo, N. Bârsan, A. Oprea, M. Sahm, T. Sahm, and U. Weimar, Appl. Phys. Lett. **85**, 2280 (2004).
[12] B. M. Warnes, F. F. Aplan, and G. Simkovich, Solid State Ionics **12**, 271 (1984).
[13] M. Radosavljevic, J. Appenzeller, P. Avouris, and J. Knoch, Appl. Phys. Lett. **84**, 3693 (2004).
[14] A. Javey, R. Tu, D. B. Farmer, J. Guo, R. G. Gordon, and H. Dai, Nano Lett. **5**, 345 (2005).
[15] R. F. G. Gardner, R. L. Moss, and D. W. Tanner, Br. J. Appl. Phys. **17**, 55 (1966).